Cortical tension regulates Hippo signaling via Par-1-mediated Kibra degradation

Sherzod A. Tokamov[1,2], Stephan Buiter[1], Anne Ullyot[1], Gordana Scepanovic[3], Audrey Miller Williams[1], Rodrigo Fernandez-Gonzalez[3], Sally Horne-Badovinac[1, 2], Richard G. Fehon[1, 2, *]

[1]Department of Molecular Genetics and Cell Biology, The University of Chicago, Chicago, IL 60637, USA

[2]Committee on Development, Regeneration, and Stem Cell Biology, The University of Chicago, Chicago, IL 60637, USA

[3]Department of Cell and Systems Biology, University of Toronto, Toronto, ON M5S 3G5, Canada

[*]Correspondence and lead contact: rfehon@uchicago.edu

Abstract
The Hippo pathway is an evolutionarily conserved regulator of tissue growth. Many Hippo signaling components have been shown to be regulated via proteolytic degradation. However, how these degradation mechanisms are themselves regulated remain unexplored. Kibra is a key upstream pathway activator that promotes its own ubiquitin-mediated degradation upon assembling a Hippo signaling complex. Here, we demonstrate that complex-dependent Kibra degradation is modulated by cortical tension. Using classical genetic, osmotic, and pharmacological manipulations of myosin activity and cortical tension, we show that increasing cortical tension leads to Kibra degradation, whereas decreasing cortical tension increases Kibra abundance. Our study also implicates Par-1 in regulating Kib abundance downstream of cortical tension. We demonstrate that Par-1 promotes ubiquitin-mediated Kib degradation in a Hippo complex-dependent manner. Furthermore, cortical tension promotes Par-1 association with the cell cortex and Par-1 is required for tension-induced Kib degradation. Collectively, our results reveal a previously unknown molecular mechanism by which cortical tension affects Hippo signaling and provide novel insights into the role of mechanical forces in growth control.

Introduction

Elucidating the mechanisms that ensure robustness and reproducibility of organ size is a fundamental problem in cell and developmental biology. A key regulator of tissue growth in animals is the Hippo pathway. At its core, the Hippo pathway consists of a kinase cascade, composed of Ser/Thr kinases Hippo (Hpo) and Warts (Wts), that phosphorylate and inhibit nuclear translocation of a pro-growth transcriptional co-activator, Yorkie (Yki). The activity of the kinase cascade is regulated by multiple upstream components, including a multivalent scaffold protein, Kibra (Kib). Kib localizes at the apical cell cortex of epithelial cells, where together with its binding partner, Merlin (Mer), it plays a key role in assembling and activating the Hippo kinase cascade to repress Yki activity. In the absence of a conventional receptor/ligand pair, however, little is known about how Kib activity is regulated.

A conserved feature of the Hippo pathway is its regulation via forces generated by F-actin and non-muscle myosin II (actomyosin). Actomyosin forces are regulated by the small GTPase RhoA (Rho1 in Drosophila), which can be activated or deactivated by guanine exchange factors (GEFs) or GTPase activating proteins (GAPs), respectively (Piekny et al., 2005). Rho1 potently stimulates actomyosin contractility by simultaneously activating Diaphanous, a formin that promotes linear F-actin bundle assembly, and Rho kinase (Rok), which phosphorylates and activates the myosin regulatory light chain (Lecuit et al., 2011). Studies over the years have shown that both F-actin polymerization and myosin activation stimulate the activity of Yki and its mammalian homologs, YAP/TAZ (Sansores-Garcia et al., 2011; Fernandez et al., 2011; Dupont et al., 2011; Wada et al., 2011; Aragona et al., 2013; Rauskolb et al., 2014; Ibar et al., 2018). Mechanistically, cytoskeletal tension was shown to promote Yki/YAP activity via LIM domain Ajuba family proteins, such as Ajuba (Jub), which accumulate at cell-cell junctions in response to tension and sequester Wts (Rauskolb et al., 2014; Pan et al., 2016; Ibar et al., 2018). However, this mechanism acts directly on the core kinase cascade, and it remains unclear whether or how tension could regulate the upstream Hippo signaling components, such as Kib.

A key determinant of Kib activity is its protein level. Loss of Kib results in tissue overgrowth via Yki activation, while the opposite occurs under ectopic Kib expression (Yu et al., 2010a; Genevet et al., 2010; Baumgartner et al., 2010; Su et al., 2017; Tokamov et al., 2021). Thus, control of Kib abundance provides an important point of dynamically modulating Kib signaling output. One way by which Kib abundance is regulated is via ubiquitin-mediated proteolytic destruction. Upon assembly if the Hippo complex, Kib is ubiquitinated via the SCF^{Slimb} E3 ubiquitin ligase and subsequently degraded (Tokamov et al., 2021). This mechanism simultaneously requires a consensus recognition motif in Kib that recruits SCF^{Slimb}, as well as the two N-terminal WW domains in Kib that mediate Hippo complex formation. Notably, Kib levels are elevated in cells with lower cortical tension, suggesting that actomyosin-generated forces could regulate Kib abundance (Tokamov et al., 2021). How Kib levels could be modulated by mechanical forces and whether this mechanism involves additional mechanosensitive components remains unknown.

In this study, using genetic, osmotic, and pharmacological manipulations of myosin activity, we report that actomyosin-generated cortical tension modulates Kib abundance. We find that increasing myosin activity and tension lowers Kib abundance, while acutely inhibiting myosin activity elevates Kib levels. Importantly, we find that tension-mediated Kib degradation occurs independently of the previously identified Jub-Wts mechanism. Instead, our results suggest that the serine/threonine kinase Par-1 promotes Kib degradation in a tension dependent manner. Together, our findings provide evidence that tension regulates upstream Hippo signaling

and advance our understanding of how mechanical forces can influence the activity of a signaling pathway.

Results

Cortical tension promotes Kib degradation

Previously, we showed that Kib's role in assembling the Hippo signaling complex promotes its own degradation, thereby forming a post-translational negative feedback loop (Tokamov et al., 2021). Additionally, our results suggested that this feedback mechanism is modulated by cortical tension because cell clones under compression display higher levels of Kib than their neighbors. To better understand how Kib abundance is regulated, we sought to genetically manipulate non-muscle myosin II (myosin) contractility as a means to affect cortical tension. To visualize Kib, we used Kib tagged with the green fluorescent protein (GFP) and expressed under the ubiquitin promoter (Ubi>Kib-GFP), a transgene that we previously showed to be an effective reporter of post-translational changes in Kib abundance (Tokamov et al., 2021). We first transiently ectopically expressed RhoGEF2 to activate Rho1 upstream of myosin in the posterior compartment of the wing imaginal disc using the *hh>Gal4* driver combined with ubiquitously expressed $Gal80^{ts}$ ($tub>Gal80^{ts}$). Strikingly, expression of RhoGEF2 for 24h resulted in a significant decrease in Kib levels (Figs. 1A-B). Using phospho-specific antibody against the phosphorylated myosin regulatory light chain (pMRLC, Zhang and Ward, 2011), we confirmed that myosin activity was upregulated under these conditions (Fig. S1A-A''). Additionally, consistent with the function of Kib in repressing Yki and the role of tension in promoting Yki transcriptional activity (Genevet et al., 2010; Yu et al., 2010b; Baumgartner et al., 2010; Rauskolb et al., 2014), we saw increased nuclear Yki accumulation upon RhoGEF2 expression (Fig. S1B-B''). In contrast, the abundance of Ubi>$Kib^{\Delta WW1}$-GFP, a variant of Kib that is insensitive to Hippo complex-mediated degradation (Tokamov et al., 2021), was not affected by RhoGEF2 expression (Figs. 1C-D). These results are consistent with our previous observation that the abundance of wild-type Kib, but not $Kib^{\Delta WW1}$, was upregulated in mosaic clones with decreased cortical tension (Tokamov et al., 2021) and suggest that cortical tension regulates Kib abundance via complex-mediated degradation.

We also previously showed that cortically localized Yki promotes myosin activation via a myosin light chain kinase called Stretchin (Strn-MLCK, Xu et al., 2018). Specifically, ectopic expression of myristoylated Yki (myr-Yki) leads to a significant increase in myosin activation. Therefore, we asked if myr-Yki expression also affected Kib levels. As with RhoGEF2 expression, ectopic myr-Yki expression substantially diminished Kib levels (Figs. 1E & F). Depletion of Strn-MLCK strongly suppressed the effect of myr-Yki, suggesting that this effect was mediated via myosin activity (Figs. 1E', F). However, Strn-MLCK depletion alone did not increase Kib levels (Fig. 1E'', F), so the physiological significance of this effect is unclear.

Changes in osmotic conditions alter myosin activity and cortical tension

Our genetic manipulations of cortical tension support the model that tension promotes Kib turnover. We sought to further test this model by acutely manipulating myosin activity and cortical tension. Changes in osmotic pressure have been used extensively to alter cortical cytoskeletal organization and tension (Di Ciano et al., 2002; Guilak et al., 2002; Sinha et al., 2011; Boulant et al., 2011; Stewart et al., 2011; Pietuch et al., 2013; Diz-Muñoz et al., 2016;

Roffay et al., 2021). Therefore, we decided to subject wing imaginal discs to different osmotic conditions (see Methods) and examine the effect on myosin activity and cortical tension. We aimed to alter medium osmolarity gently enough to avoid cell death or tissue rupture and ensure reversibility of the effected changes.

We first examined the effect of different osmotic conditions on myosin activity using the anti-pMRLC antibody. Compared to isotonic controls, we saw a slight decrease in pMRLC staining under hypertonic conditions and a substantial increase in pMRCL under hypotonic conditions (Figs. 2A-C'), indicating that osmotic manipulations can acutely alter myosin activation. To ask if the observed changes in myosin activity affected cortical tension, we performed laser-cutting experiments on individual bicellular junctions and measured their initial recoil velocity. Because of the inherent heterogeneity of cell junctional lengths and apical areas across the wing imaginal epithelium, we restricted all laser cuts to the ventral-anterior region of the presumptive wing blade, which normally contains cells with larger apical areas and longer junctions. Additionally we were careful to avoid proximity to mitotic cells (Fig. S2A). Consistent with the observed differences in pMRLC staining, we saw a mild, but significant, decrease in recoil velocities under hypertonic conditions and a profound increase in recoil upon hypotonic shift (Figs. 2D-E, Movie 1). Importantly, there was no correlation between junctional recoil and the initial junction length (Fig. S2B). Collectively, these results show that osmotic manipulations can be used to acutely modulate myosin activity and cortical tension in the imaginal epithelium.

To further validate that osmotic shifts can be used to induce functional changes in tension, we examined the localization of Yki-YFP. Because tension is known to promote nuclear Yki accumulation, we hypothesized that hypertonic conditions (lower tension) should lead to less nuclear Yki, while hypotonic conditions should result in more nuclear Yki. For these experiments, in order to see a definitive effect on Yki localization, we increased the incubation time to 30 min. Consistent with our hypothesis, shifting tissues from an isotonic to a hypertonic solution resulted in a decrease in nuclear Yki (Figs. S4A-B'', D). Conversely, shifting to a hypotonic solution led to a dramatic increase in nuclear Yki (Figs. S4C-D). To further demonstrate the significance of this effect, we decided to first concentrate Yki in the nuclei under hypotonic conditions and then shift to a hypertonic environment. Hypotonically-induced nuclear Yki accumulation was completely reversed after incubation in a hypertonic solution (Fig. S4E-G''). Together, these results show that osmotic manipulations can be used to acutely modulate myosin activity and cortical tension in an epithelial monolayer with biologically relevant consequences.

Osmotic shifts affect Kib abundance

Given our result that changes in the medium osmolarity can influence cortical tension, we asked if the osmotic manipulations also affected Kib abundance. Compared to isotonic conditions, incubating tissues in a hypertonic solution resulted in an increased Kib abundance at the apical cortex (Figs. 3A, B, & D). Moreover, Kib fluorescence also increased in more basal tissue sections, suggesting that the apical increase in Kib was not due to apical recruitment from the cytoplasmic pool (Fig. 3E). Conversely, in tissues incubated in a hypotonic solution, Kib abundance decreased dramatically both at the apical cortex and in more basal tissue sections compared to isotonic controls (Figs. 3C-E). In contrast, fluorescence intensity of Ubi>Kib$^{\Delta WW1}$-GFP and Ecad-mKate2 did not change significantly under osmotic shifts (Figs.S3A-C, 3F). These results demonstrate that cortical tension can rapidly modulate Kib abundance.

We also considered the possibility that changes in apical area could alter Kib distribution and fluorescence intensity by concentrating or diluting the protein at the cortex. To address this possibility, we measured apical cell areas upon subjecting wing imaginal tissues to hypotonic or hypertonic conditions. Immediately after the addition of the hypotonic solution, apical areas increased rapidly during the first ~3 min of incubation (Fig. 3G). However, this initial increase was followed by a steady decrease of areas in the next 12 min, until on average the areas returned roughly to their initial values (Fig. 3G, Movie 2). Similarly, addition of the hypertonic solution resulted in a transient reduction in apical areas during the first ~3 min, followed by a steady return to their starting values by 15 min of incubation (Fig. 3H, Movie 3). Because we measured Kib fluorescence after 15 min of incubation, changes in apical area are unlikely to explain the observed changes in cortical Kib abundance under osmotic shifts. These results suggest that changes in myosin activity may be responsible for changes in Kib abundance under osmotic shifts.

Inhibition of myosin activity blocks Kib degradation under hypotonic shift

If the changes in Kib levels under osmotic shifts require myosin activity, as expected if cortical tension regulates Kib abundance, then blocking myosin activity under hypotonic conditions should block Kib degradation. To test this idea, we used Y-27632, a pharmacological inhibitor of Rho kinase (Rok) activity (Uehata et al., 1997). Under isotonic conditions, we observed a slight reduction in pMRLC staining when tissues were treated with Y-27632 (Fig. 4A-B'), though this effect was not statistically significant (Fig. 4I). However, Y-27632 potently inhibited myosin hyperactivation induced by hypotonic conditions (Figs. 4C-D', I).

We next asked if Y-27632 treatment would affect Kib abundance. Strikingly, we observed a substantial increase in Kib abundance after 15 min of Y-27632 treatment under isotonic conditions (Figs. 4E, F, & J), supporting the idea that myosin activity promotes Kib degradation. To test if Rok inhibition could block the effect of hypotonic conditions, we first incubated our tissues in hypotonic medium for 15min and then treated them with Y-27632, still in hypotonic medium. Treatment with Y-27632 strongly reversed the effect of the hypotonic medium on Kib abundance (Figs. 4G, H, & J), suggesting that the effect of osmotic shifts on Kib abundance is caused by cortical tension.

We also considered the possibility that the effect of Y-27632 could be mediated via inhibition of another known target of this inhibitor, the atypical protein kinase C (aPKC). To test this possibility, we took advantage of a conditional allele of aPKC, *aPKC*^{as4}, which can be acutely inhibited using 1NA-PP1, an allele-specific analog of a potent kinase inhibitor (Hannaford et al., 2019a). As expected, under normal conditions, aPKC^{as4} was enriched at the apical cortex in the wing imaginal epithelium (Fig. S5A-A'). In contrast, treatment with 1NA-PP1 severely inhibited aPKC cortical localization (Figs. S5B-B'). On the other hand, treatment with Y-27632 did not significantly affect aPKC cortical localization in wild type imaginal discs (Figs. S5C-D'). Additionally, we treated wing discs homozygous for *aPKC*^{as4} allele with 1NA-PP1 and did not observe any changes in Kib abundance upon aPKC inhibition (Figs. S5E-G). Collectively, these results show that the effect of Y-27632 on Kib abundance is not due to inhibition of aPKC.

Par-1 regulates Kib abundance

How can tension influence abundance of a signaling protein such as Kib? Previous work identified a mechanism whereby tension inhibits Hippo signaling via Jub-mediated sequestration

and inactivation of Wts/LATS at the cell-cell junctions (Rauskolb et al., 2014; Ibar et al., 2018). However, there are three lines of evidence that suggest that tension-mediated regulation of Kib levels does not occur through the Jub-Wts mechanism. First, because we showed previously that Wts promotes Kib degradation (Tokamov et al., 2021), the decrease in Kib levels under higher cortical tension is unlikely to be explained by Jub-mediated Wts sequestration. Second, although we see a significant increase in myosin activity under hypotonic conditions (Fig. 2C), we do not detect significant changes in cortical Jub levels under osmotic manipulations (Figs. S6A-D). Third, loss of Jub does not affect Kib levels (Fig. S6E).

Recently, myosin activity was shown to promote cortical localization of Par-1 in the Drosophila oocyte (Doerflinger et al., 2021). Interestingly, Par-1 mediates proteolytic degradation of an SCF^{Slimb} substrate Oskar (Morais-de-Sá et al., 2013) and is known to physically associate with Hippo signaling components and regulate tissue growth (Huang et al., 2013, p. 1). We therefore hypothesized that cortical tension could promote Kib degradation via Par-1. To test this idea, first we asked if Par-1 regulates Kib abundance using Ubi>Kib-GFP as a reporter. Kib levels increased significantly upon Par-1 depletion (Figs. 5A & C, S7A), whereas ectopic Par-1 expression resulted in a significant reduction in Kib levels (Figs. 5B & C). In contrast, loss of Par-1 did not affect abundance of $Kib^{\Delta WW1}$ (Figs. 5D & E), suggesting that Kib-mediated Hippo complex assembly is necessary for Par-1 regulation of Kib abundance (Tokamov et al., 2021).

Par-1 was previously shown to inhibit Hpo activity by direct phosphorylation on Ser30, which prevents Hpo association with Sav (Huang et al., 2013). Therefore, we considered the possibility that the increase in Kib abundance under loss of Par-1 was indirectly caused by the lack of Hpo phosphorylation on Ser30. If this were the case, we reasoned that ectopic expression of Hpo construct that is refractory to Par-1 phosphorylation (Hpo^{S30A}), would also lead to increased Kib abundance. To this end, we first transiently expressed wild-type Hpo in the posterior compartment of the wing imaginal disc and examined the effect on Kib levels. Consistent with our previous finding that Hpo promotes Kib ubiquitination and degradation (Tokamov et al., 2021), Kib levels decreased significantly under ectopic Hpo expression (Fig. S7B). Importantly, ectopic expression of Hpo^{S30A} still induced a decrease in Kib abundance (Fig. S7C), suggesting that the effect of Par-1 on Kib abundance is not mediated through Hpo phosphorylation.

We have previously shown that Kib is ubiquitinated via SCF^{Slimb} in cultured Schneider's 2 (S2) cells. Because Par-1 is a kinase and is known to function with SCF^{Slimb}, we asked if Par-1 affects Kib ubiquitination or phosphorylation in S2 cells. Significantly, while Kib was ubiquitinated in control cells, Par-1 depletion led to a strong decrease in Kib ubiquitination (Fig. 5F). To test if Par-1 promotes Kib phosphorylation, we performed gel-shift assays in the presence of wild type or kinase-dead Par-1 ($Par\text{-}1^{KD}$). As previously observed in gel-shift assays in vivo, Kib is normally phosphorylated in S2 cells, as it appears as a smeary, slow migrating band that collapses into a single, faster migrating band with phosphatase treatment (Fig. 5G, Tokamov et al., 2021). Addition of active Par-1, but not $Par\text{-}1^{KD}$, resulted in a upward shift of Kib band and disappearance of the lower, non-phosphorylated pool, suggesting that Par-1 promotes Kib phosphorylation (Fig. 5G). Together, these results suggest that Par-1 regulates ubiquitin-mediated Kib degradation and that tension could modulate Kib abundance via Par-1.

Cortical tension promotes Par-1 association with the cortex
Given the previous report that myosin activity promotes cortical Par-1 localization in the *Drosophila* oocyte (Doerflinger et al., 2021), we wondered if a similar effect could be observed in the wing imaginal epithelium. To this end, we first examined Par-1 localization in control cells or in cells overexpressing RhoGEF2. Although known as a basolateral component, in the Drosophila blastoderm Par-1 also localizes at the apicolateral cortex (Bayraktar et al., 2006). In the wing imaginal disc, Par-1 displayed apical and basolateral localization, though its localization appeared diffused in both places (Fig. 6A & A'). Transient overexpression of RhoGEF2 resulted in sharper Par-1 localization at the cell cortex both apically and basolaterally (Fig. 6B & B'), suggesting that tension can affect Par-1 cortical association. As an alternative approach, we also examined Par-1 localization using Airyscan confocal microscopy (to enhance signal and resolution) under hypoosmotic conditions. Similar to ectopic RhoGEF2 expression, Par-1 was more tightly associated with the apical and basolateral cortex under hypotonic compared to isotonic conditions (Figs. 6C-D'). These results suggest that tension promotes Par-1 association with the cell cortex.

Par-1 is required for tension-dependent degradation of Kib
We reasoned that if tension regulates in Kib abundance via Par-1, then in the absence of Par-1 tension would have no effect on Kib levels. To test this idea, we depleted Par-1 in the posterior compartment of the wing imaginal disc using the *hh>Gal4* driver and quantified changes in Kib levels when tissues were shifted from isotonic to hypotonic conditions. While we observed a significant decrease in Kib intensity in the anterior (control) compartment, there was no significant change in the posterior (Par-1 depleted) compartment (Figs. 6E-G). Collectively, these results are consistent with the idea that tension modulates Kib abundance by controlling Par-1 cortical association.

Discussion
Elucidating the molecular mechanisms that control the abundance of individual signaling components has been central to our understanding how the Hippo pathway is regulated (Ribeiro et al., 2014; Bosch et al., 2014; Rodrigues-Campos and Thompson, 2014; Aerne et al., 2015; Ma et al., 2018; Fulford et al., 2019; Wang et al., 2019; Misra and Irvine, 2019; Tokamov et al., 2021). However, how these different mechanisms themselves are regulated has been a poorly understood and intriguing area of investigation. Our work reveals a previously unrecognized role of cortical tension in modulating the abundance of a key upstream Hippo pathway component, Kib. Using a combination of genetic, osmotic, and pharmacological approaches, we demonstrate that cortical tension promotes Kib degradation. Our study also implicates Par-1 in mediating Kib degradation downstream of cortical tension. This work advances our understanding of how tension regulates Hippo signaling and advances our understanding of the role of mechanical forces in tissue growth and patterning.

We provide several lines of evidence that Kib is degraded as a result of myosin-generated tension. First, we show that activation of myosin via two different myosin light chain kinases, Rok (in the case of ectopic RhoGEF2 expression and Y-27632 treatment) and Strn-MLCK (in the case of ectopic myr-Yki expression) decreases Kib abundance (Figs. 1 & 4), suggesting that Kib degradation occurs irrespective of the upstream mechanisms of myosin activation. Second, although RhoGEF2 is known to promote both myosin activity and formin-mediated F-actin

assembly, we did not observe a detectible effect on F-actin under transient RhoGEF2 expression, whereas myosin activity was substantially upregulated (Fig. S1). Third, we develop a simple, non-genetic and acute approach to dramatically increase myosin activity using hypotonic conditions and demonstrate that myosin activation using this method results in Kib degradation (Figs. 2-4). Thus, we propose that Kib degradation is modulated by cortical tension downstream of myosin activity.

Our results also suggest that Kib degradation downstream of cortical tension is mediated via Hippo complex formation. We have shown previously that Kib targets itself for ubiquitin-mediated degradation upon Hippo complex assembly, and this process requires Kib's WW1 domain and a consensus degron motif recognized by the E3 ubiquitin ligase $SCF^{Slimb/\beta TrCP}$ (Tokamov et al., 2021). In this study, we observe that the abundance of wild-type Kib, but not $Kib^{\Delta WW1}$, is modulated via myosin activity, raising the question of how tension can promote complex-dependent Kib turnover. In the simplest scenario, cortical tension could promote the association of existing Kib complexes with a tension-sensitive component capable of modulating Kib levels. We identify Par-1 as a potential link in this process. Myosin activity was previously reported to promote cortical Par-1 localization in the *Drosophila* oocyte (Doerflinger et al., 2021). Here, we show that Par-1 promotes turnover of wild-type Kib, but not $Kib^{\Delta WW1}$, in vivo and regulates Kib phosphorylation and ubiquitination in cultured cells (Fig. 5). Importantly, cortical tension fails to induce Kib turnover in cells depleted of Par-1 (Fig. 6). Based on these results, and our observations that Par-1 becomes more tightly associated with the cell cortex under increased cortical tension (Fig. 6), we propose that cortical tension could regulate Kib levels at least in part by modulating the association of Par-1 with Kib signaling complexes. Interestingly, a recent study in human cells also suggested that tension generated at the ECM promotes degradation of a Hpo homolog, MST2, by modulating the physical interaction between MST2 and $SCF^{Slimb/\beta TrCP}$ complex (Fiore et al., 2022). Thus, in a more complex scenario, cortical tension could also regulate Kib association with multiple components of the degradation machinery, including $SCF^{Slimb/\beta TrCP}$.

This study also highlights the recurring role of Par-1 in the regulation of Hippo signaling. Previous work suggested that Par-1 phosphorylates Hpo, which prevents Hpo association with Sav (Huang et al., 2013). Here, we find that Par-1 regulates Kib abundance independently of Hpo phosphorylation. Our observation that Par-1 regulates the abundance of wild-type Kib but not $Kib^{\Delta WW1}$ suggests that Par-1 regulates Kib via the Hippo complex-mediated degradation mechanism involving $SCF^{Slimb/\beta TrCP}$ (Tokamov et al., 2021). This idea is supported by a previous report that Par-1 functions with $SCF^{Slimb/\beta TrCP}$ in promoting turnover of Oscar during Drosophila oocyte development (Morais-de-Sá et al., 2013). Notably, active Par-1 was also found to be a target of $SCF^{Slimb/\beta TrCP}$-mediated degradation (Lee et al., 2012), further highlighting the tight association between Par-1, $SCF^{Slimb/\beta TrCP}$, and Kib. It is still unclear what happens to the rest of the Hippo signaling complex after Kib is degraded, but the multifaceted function of Par-1 in inhibiting Hpo activity, Hpo-Sav interaction, and promoting Kib degradation could provide the means of dissociating the entire signaling complex upon Kib turnover.

One of the surprising observations in our study is that while cortical tension induced by hypotonic conditions triggers Kib degradation, it does not affect cortical accumulation of Jub. Previous work has shown that increasing myosin activity via genetic manipulations enhances Jub accumulation at the adherens junctions, where Jub sequesters Wts (Rauskolb et al., 2014). This enhanced junctional accumulation is thought to be mediated via tension-induced opening of α-catenin conformation, which exposes a region in α-catenin responsible for Jub recruitment

(Rauskolb et al., 2014; Alégot et al., 2019; Sarpal et al., 2019). Combined with these reports, our observations suggest that hypotonically-induced myosin activation may differ from that achieved via common genetic manipulations. Most obviously, this difference could be temporal – hypotonic treatment of wing imaginal discs induces dramatic myosin activation and Kib degradation within 15 minutes (Fig. 2), whereas genetic manipulations are done in the order of hours or days. Thus, it is possible that α-catenin-mediated recruitment of Jub occurs at a longer timescale compared to the more dynamic Kib turnover. Counter to this argument, however, a recent study observed rapid junctional accumulation of Jub-Wts clusters at sites of high tension in the Drosophila developing notum (López-Gay et al., 2020). An alternative explanation is that hypotonically-induced myosin activation does not result in α-catenin conformational changes. The opening of α-catenin conformation along bicellular junctions is thought to be triggered via actomyosin forces applied orthogonal to the junctions (Rauskolb et al., 2019; López-Gay et al., 2020). This is unlikely to be the case under hypotonic conditions, where actomyosin generated forces would be generated parallel to the membrane to counteract the mechanical stretching induced by hydrostatic pressure. In contrast, myosin-dependent Par-1 recruitment to the cell cortex is thought to depend on MRLC phosphorylation, whereby di-phosphorylated, but not mono-phosphorylated MRLC recruits Par-1. Therefore, unlike the Jub-Wts mechanism, Kib degradation mechanism we report here could respond directly to biochemical changes in myosin activity rather than to the resultant increased cortical tension.

Finally, our study raises the question of the biological importance of tension-dependent Kib degradation. In the growing wing imaginal epithelium, cortical tension was shown to be higher at the tissue periphery than at the tissue center (LeGoff et al., 2013; Mao et al., 2013). Greater tension at the periphery was proposed to drive growth, possibly via Yki activity, to compensate for the lower concentration of growth-stimulating morphogens, which diffuse from narrow stripes of cells at the center of the tissue (Aegerter-Wilmsen et al., 2007, 2012; Hariharan, 2015; Pan et al., 2016). Additionally, we have previously reported that Kib degradation occurs more prominently at the tissue periphery, where cortical tension is higher (Tokamov et al., 2021). Based on these studies, we propose that tension-mediated Kib degradation could serve to pattern Hippo signaling activity, and therefore growth, across a growing epithelium such as the wing imaginal disc. How Kib degradation and other tension-regulated mechanisms, such as the Jub-Wts mechanism, are coordinated to control the Hippo pathway and growth remains a challenging question in the field. However, we believe this study provides valuable insights for future investigation of the molecular mechanisms by which mechanical forces affect tissue growth.

Methods

Table 1: Reagents

Reagent type (species) or resource	Designation	Source or reference	Identifiers	Additional information
genetic reagent (*D. melanogaster*)	*Ubi>Kib-GFP-FLAG*	(Tokamov et al., 2021)		
genetic reagent (*D. melanogaster*)	*Ubi-Kib$^{\Delta WW1}$-GFP-FLAG*	(Tokamov et al., 2021)		
genetic reagent (*D. melanogaster*)	*UASp-T7-RhoGEF2*	Bloomington Drosophila Stock Center	BL9387	
genetic reagent (*D. melanogaster*)	*UASt-myr-Yki*	10.1016/j.devcel.2018.06.017		
genetic reagent (*D. melanogaster*)	*UAS-Strn RNAi*	Bloomington Drosophila Stock Center	BL26736	Validated in 10.1016/j.devcel.2018.06.017
genetic reagent (*D. melanogaster*)	*UAS-Par-1 RNAi*	Bloomington Drosophila Stock Center	BL32410	
genetic reagent (*D. melanogaster*)	*UAS-jub RNAi*	Bloomington Drosophila Stock Center	BL30806	Validated in 10.1016/j.cub.2010.02.035
genetic reagent (*D. melanogaster*)	*Ecad-3XmKate2*	(Pinheiro et al., 2017)		

genetic reagent (*D. melanogaster*)	*Par-1:GFP (protein trap)*	Bloomington Drosophila Stock Center	BL64452	
genetic reagent (*D. melanogaster*)	*Jub:GFP*	Bloomington Drosophila Stock Center	BL56806	
genetic reagent (*D. melanogaster*)	w^{1118};yki^{B5} {*yki-YFP*} *VK37*	(Xu et al., 2018)		
genetic reagent (*D. melanogaster*)	$aPKC^{as4}$	(Hannaford et al., 2019b)		
Antibody	anti-pSqh (Guinea pig, polyclonal)	(Zhang and Ward, 2011)		Tissue staining (1:300)
Antibody	anti-DEcad (Rat, polyclonal)	Developmental Studies Hybridoma Bank	Cat#AB_528120; RRID:AB_528120	Tissue staining (1:1000)
Antibody	anti-PKC, rabbit polyclonal	Santa Cruz Biotechnology	Lot#: G2304	tissue staining (1:1000)
Antibody	anti-GFP, guinea pig, polyclonal	(Yee et al., 2019)		IP (1:1250)
Antibody	anti-GFP, rabbit, polyclonal	Michael Glotzer, (University of Chicago)		IB (1:5000)
Chemical	Y-27632	Fisher Scientific	Cat. # 12541	Rho kinase inhibitor

Chemical	1-NA-PP1	Cayman	Cat. # CAYM-10954-1	ATP analog

***Drosophila* husbandry**

Drosophila melanogaster was cultured using standard techniques at 25°C (unless otherwise noted). For Gal80^{ts} experiments, crosses were maintained at 18°C until larvae reached late second or early third instar stages and shifted to 29°C for the duration specified in each experiment. Immediately after incubation at 29°C, wing imaginal tissues were dissected from wandering third instar larvae and imaged live.

Live imaging

Live imaging method of the wing imaginal discs was adapted from Restrepo et al. (2016). Briefly, wing imaginal tissues were first dissected in Schneider's Drosophila Medium (Sigma) supplemented with 10% Fetal Bovine Serum (Thermo Fisher Scientific) on a siliconized glass slide. The tissues were then transferred with a pipette in 5-10µl of medium to a glass bottom microwell dish (MatTek, 35mm petri dish, 14mm microwell) with No. 1.5 coverglass. The discs were oriented so that the apical side of the disc proper faced the coverglass. A Millicell culture insert (Sigma, 12mm diameter, 8µm membrane pore size) was prepared in advance by cutting off the bottom legs with a razor blade and removing any excess membrane material around the rim of the insert. The insert was carefully placed into the 14mm microwell space, directly on top of the drop containing properly oriented tissues. To prevent the tissue from moving, the space between the insert and the microwell was sealed with ~15µl of mineral oil. Media with indicated osmolarity and/or chemical inhibitor was then added into the chamber of the insert (200µl in all experiments). An inverted Zeiss LSM880 laser scanning confocal microscope equipped with a GaAsP spectral detector and the Airyscan module was used for all imaging (except for laser ablation experiments, see below).

Osmotic shift experiments

Schneider's Drosophila Medium (Sigma) supplemented with 10% Fetal Bovine Serum (Thermo Fisher Scientific) was used as isotonic medium (~360mOsm). To make a hypertonic solution, the osmolarity of the isotonic solution was increased to 460mOsm using 1M NaCl. To make a hypotonic solution, the isotonic medium was diluted with deionized water to 216mOsm. All osmotic solutions were prepared fresh immediately before the experiments. In most experiments, tissues were incubated for 15 min. For practical reasons, in laser ablation experiments tissues were incubated for 8 min to allow for measurements to be taken at an average of 15 min under osmotic incubations. To observe changes in Yki-YFP localization, tissues were incubated for 30min.

pSqh staining experiments

During experiments, wandering third instar larvae were dissected in an isotonic solution and the wing imaginal discs were transferred into a 150µl drop of prepared osmotic medium. For experiments with Y-27632, osmotic media with 50µM of Y-27632 were prepared. The tissues

were incubated for 15 min. After incubation, the discs were washed with 1X Ringer's buffer with correspondingly adjusted osmolarity (i.e. for hypertonic experiments, a hypertonic wash was prepared the same way as described above, except 1X Ringer's was used instead of the Schneider's medium) and fixed for 20 min in 2% paraformaldehyde/1X Ringer's solution also with properly adjusted osmolarity (for Y-27632 experiments, 50μM of Y-27632 was also added in the wash and the fix solutions). Tissues were then stained as previously described (McCartney and Fehon, 1996).

Laser ablation experiments

Laser cuts were conducted using a pulsed Micropoint nitrogen laser (Andor Technology) tuned to 365 nm and mounted on an Andor Revolution XD spinning disk confocal microscope. Individual junctions were ablated by delivering 3 pulses at a single point with a duration of 67 ms/pulse. The tissue was imaged 2x before and 20x immediately after ablation, with a time interval of 4 s. Images were acquired using a 100X oil-immersion lens (Olympus, NA 1.40), an iXon Ultra 897 camera (Andor), and Metamorph (Molecular Devices) as the image acquisition software. Sixteen-bit Z-stacks were collected at each time point consisting of 7 slices with 0.5 μm interval.

To measure initial recoil velocity, the positions of the two tricellular vertices connected by the ablated junction were manually tracked using the SIESTA image analysis platform (Fernandez-Gonzalez and Zallen, 2011), and the initial retraction velocities were calculated using custom MATLAB scripts.

Image analysis, quantification of fluorescence intensities and apical areas

All images were processed in ImageJ. Mean fluorescence intensity measurements were taken from maximum apical projections (~0.75 μm/section, four to six sections) or from single basal optical sections (~7.5-10μm below the apical surface). Plots and statistical analyses of mean fluorescence intensities were generated using GraphPad Prism software.

To measure changes in apical areas under osmotic shifts, cells were segmented using Cellpose (Stringer et al., 2021) and tracked via a tracking algorithm previously described (Williams et al., 2022). Only the cells that remained in the field of view for the entire duration of the movies were used for quantification. Areas and the corresponding standard error values were plotted using Matplotlib library in Python.

Detection of Kibra ubiquitination in S2 cells

Kibra ubiquitination assay was performed as described previously (Tokamov et al., 2021). Briefly, 3.5 x 10^6 S2 cells (S2-DGRC) were transfected with a total of 500 ng of indicated DNA using dimethyldioctadecylammonium bromide (Sigma; Han, 1996) at 250 mg/ml in six-well plates.

pMT-Kib-GFP was co-transfected with pMT-HA-Ub (Zhang et al., 2006) where indicated to provide labeled ubiquitin. To induce expression of the pMT constructs, 700 mM CuSO4 was added to the wells 24 hr prior to cell lysis (2 days after transfection)To inhibit proteasomal degradation, 50 mM MG132 (Cayman Chemical) and 50 mM calpain inhibitor I (Sigma Aldrich) was added 4 hr prior to cell lysis. Cells were lysed in RIPA buffer (150 mM NaCl, 1% NP-40, 0.5% Na deoxycholate, 0.1% SDS, and 25 mM Tris [50 mM, pH 7.4]), supplemented with 5 mM N-ethylmaleimide and Complete protease inhibitor cocktail (Roche, one tablet/10 ml of buffer). HA-tagged ubiquitin was purified using Pierce anti-HA magnetic beads (clone 2–2.2.14). Lysates

and IP samples were run on 8% polyacrylamide gel and ubiquitinated Kib in the IP samples was detected by Western Blot using anti-GFP antibody (rabbit, see Table 1).

Detection of Kibra phosphorylation in S2 cells

pMT-Kib-GFP and pAHW-Par-1 or pAHW-Par-1^{KD} (gift from Bingwei Lu, Stanford University) were transfected and expression was induced as described above. Immunoprecipitation (IP) was performed 3 days after transfection. To induce expression of pMT-Kib-GFP, 700 mM CuSO4 was added to the wells 24 hr prior to cell lysis (2 days after transfection).

Cells were harvested and lysed on ice in buffer containing 25 mM Hepes, 150 mM NaCl, 1 mM ethylenediaminetetraacetic acid, 0.5 mM ethylene glycol-bis(b-aminoethyl ether)-N,N,N0,N0-tetraacetic acid, 0.9 M glycerol, 0.1% Triton X-100, 0.5 mM Dithiothreitol, and Complete protease inhibitor (Roche) and PhosSTOP (Sigma Aldrich) phosphatase inhibitor cocktails at one tablet/10 ml concentration each. Cell lysates were then incubated with anti-GFP antibody (guinea pig, see Table 1) for 30min. Antibody-bound Kib-GFP was pulled down using Pierce Protein A magnetic beads (Thermo Scientific) for 1.5h. A control immunoprecipiated sample was treated with λ-phosphatase. Samples were run on 8% polyacrylamide gel, with 118:1 acrylamide/bisacrylamide (Scheid et al., 1999), to better resolve phosphorylated Kib species. Kib was detected by Western Blot using anti-GFP antibody (rabbit, see Table 1).

References

Aegerter-Wilmsen, T., Aegerter, C.M., Hafen, E., Basler, K., 2007. Model for the regulation of size in the wing imaginal disc of Drosophila. Mechanisms of Development 124, 318–326. https://doi.org/10.1016/j.mod.2006.12.005

Aegerter-Wilmsen, T., Heimlicher, M.B., Smith, A.C., de Reuille, P.B., Smith, R.S., Aegerter, C.M., Basler, K., 2012. Integrating force-sensing and signaling pathways in a model for the regulation of wing imaginal disc size. Development 139, 3221–3231. https://doi.org/10.1242/dev.082800

Aerne, B.L., Gailite, I., Sims, D., Tapon, N., 2015. Hippo Stabilises Its Adaptor Salvador by Antagonising the HECT Ubiquitin Ligase Herc4. PLOS ONE 10, e0131113. https://doi.org/10.1371/journal.pone.0131113

Alégot, H., Markosian, C., Rauskolb, C., Yang, J., Kirichenko, E., Wang, Y.-C., Irvine, K.D., 2019. Recruitment of Jub by α-catenin promotes Yki activity and *Drosophila* wing growth. Journal of Cell Science 132, jcs222018. https://doi.org/10.1242/jcs.222018

Aragona, M., Panciera, T., Manfrin, A., Giulitti, S., Michielin, F., Elvassore, N., Dupont, S., Piccolo, S., 2013. A Mechanical Checkpoint Controls Multicellular Growth through YAP/TAZ Regulation by Actin-Processing Factors. Cell 154, 1047–1059. https://doi.org/10.1016/j.cell.2013.07.042

Baumgartner, R., Poernbacher, I., Buser, N., Hafen, E., Stocker, H., 2010. The WW Domain Protein Kibra Acts Upstream of Hippo in Drosophila. Developmental Cell 18, 309–316. https://doi.org/10.1016/j.devcel.2009.12.013

Bayraktar, J., Zygmunt, D., Carthew, R.W., 2006. Par-1 kinase establishes cell polarity and functions in Notch signaling in the *Drosophila* embryo. Journal of Cell Science 119, 711–721. https://doi.org/10.1242/jcs.02789

Bosch, J.A., Sumabat, T.M., Hafezi, Y., Pellock, B.J., Gandhi, K.D., Hariharan, I.K., 2014. The Drosophila F-box protein Fbxl7 binds to the protocadherin Fat and regulates Dachs localization and Hippo signaling. eLife 3, e03383. https://doi.org/10.7554/eLife.03383

Boulant, S., Kural, C., Zeeh, J.-C., Ubelmann, F., Kirchhausen, T., 2011. Actin dynamics counteract membrane tension during clathrin-mediated endocytosis. Nat Cell Biol 13, 1124–1131. https://doi.org/10.1038/ncb2307

Di Ciano, C., Nie, Z., Szászi, K., Lewis, A., Uruno, T., Zhan, X., Rotstein, O.D., Mak, A., Kapus, A., 2002. Osmotic stress-induced remodeling of the cortical cytoskeleton. American Journal of Physiology-Cell Physiology 283, C850–C865. https://doi.org/10.1152/ajpcell.00018.2002

Diz-Muñoz, A., Thurley, K., Chintamen, S., Altschuler, S.J., Wu, L.F., Fletcher, D.A., Weiner, O.D., 2016. Membrane Tension Acts Through PLD2 and mTORC2 to Limit Actin Network Assembly During Neutrophil Migration. PLoS Biol 14, e1002474. https://doi.org/10.1371/journal.pbio.1002474

Doerflinger, H., Zimyanin, V., St Johnston, D., 2021. The Drosophila anterior-posterior axis is polarized by asymmetric myosin activation. Current Biology S0960982221015487. https://doi.org/10.1016/j.cub.2021.11.024

Dupont, S., Morsut, L., Aragona, M., Enzo, E., Giulitti, S., Cordenonsi, M., Zanconato, F., Le Digabel, J., Forcato, M., Bicciato, S., Elvassore, N., Piccolo, S., 2011. Role of YAP/TAZ in mechanotransduction. Nature 474, 179–183. https://doi.org/10.1038/nature10137

Fernandez, B.G., Gaspar, P., Bras-Pereira, C., Jezowska, B., Rebelo, S.R., Janody, F., 2011. Actin-Capping Protein and the Hippo pathway regulate F-actin and tissue growth in Drosophila. Development 138, 2337–2346. https://doi.org/10.1242/dev.063545

Fiore, A.P.Z.P., Rodrigues, A.M., Ribeiro-Filho, H.V., Manucci, A.C., de Freitas Ribeiro, P., Botelho, M.C.S., Vogel, C., Lopes-de-Oliveira, P.S., Pagano, M., Bruni-Cardoso, A., 2022. Extracellular matrix stiffness regulates degradation of MST2 via SCF βTrCP. Biochimica et Biophysica Acta (BBA) - General Subjects 1866, 130238. https://doi.org/10.1016/j.bbagen.2022.130238

Fulford, A.D., Holder, M.V., Frith, D., Snijders, A.P., Tapon, N., Ribeiro, P.S., 2019. Casein kinase 1 family proteins promote Slimb-dependent Expanded degradation. eLife 8, e46592. https://doi.org/10.7554/eLife.46592

Genevet, A., Wehr, M.C., Brain, R., Thompson, B.J., Tapon, N., 2010. Kibra Is a Regulator of the Salvador/Warts/Hippo Signaling Network. Developmental Cell 18, 300–308. https://doi.org/10.1016/j.devcel.2009.12.011

Guilak, F., Erickson, G.R., Ting-Beall, H.P., 2002. The Effects of Osmotic Stress on the Viscoelastic and Physical Properties of Articular Chondrocytes. Biophysical Journal 82, 720–727. https://doi.org/10.1016/S0006-3495(02)75434-9

Hannaford, M., Loyer, N., Tonelli, F., Zoltner, M., Januschke, J., 2019a. A chemical-genetics approach to study the role of atypical protein kinase C in *Drosophila*. Development dev.170589. https://doi.org/10.1242/dev.170589

Hannaford, M., Loyer, N., Tonelli, F., Zoltner, M., Januschke, J., 2019b. A chemical-genetics approach to study the role of atypical protein kinase C in *Drosophila*. Development dev.170589. https://doi.org/10.1242/dev.170589

Hariharan, I.K., 2015. Organ Size Control: Lessons from Drosophila. Developmental Cell 34, 255–265. https://doi.org/10.1016/j.devcel.2015.07.012

Huang, H.-L., Wang, S., Yin, M.-X., Dong, L., Wang, C., Wu, W., Lu, Y., Feng, M., Dai, C., Guo, X., Li, L., Zhao, B., Zhou, Z., Ji, H., Jiang, J., Zhao, Y., Liu, X.-Y., Zhang, L., 2013. Par-1 Regulates Tissue Growth by Influencing Hippo Phosphorylation Status and Hippo-Salvador Association. PLoS Biology 11, e1001620. https://doi.org/10.1371/journal.pbio.1001620

Ibar, C., Kirichenko, E., Keepers, B., Enners, E., Fleisch, K., Irvine, K.D., 2018. Tension-dependent regulation of mammalian Hippo signaling through LIMD1. J Cell Sci 131, jcs214700. https://doi.org/10.1242/jcs.214700

Lecuit, T., Lenne, P.-F., Munro, E., 2011. Force Generation, Transmission, and Integration during Cell and Tissue Morphogenesis. Annu. Rev. Cell Dev. Biol. 27, 157–184. https://doi.org/10.1146/annurev-cellbio-100109-104027

Lee, S., Wang, J.-W., Yu, W., Lu, B., 2012. Phospho-dependent ubiquitination and degradation of PAR-1 regulates synaptic morphology and tau-mediated Aβ toxicity in Drosophila. Nat Commun 3, 1312. https://doi.org/10.1038/ncomms2278

LeGoff, L., Rouault, H., Lecuit, T., 2013. A global pattern of mechanical stress polarizes cell divisions and cell shape in the growing *Drosophila* wing disc. Development 140, 4051–4059. https://doi.org/10.1242/dev.090878

López-Gay, J.M., Nunley, H., Spencer, M., di Pietro, F., Guirao, B., Bosveld, F., Markova, O., Gaugue, I., Pelletier, S., Lubensky, D.K., Bellaïche, Y., 2020. Apical stress fibers enable a scaling between cell mechanical response and area in epithelial tissue. Science 370, eabb2169. https://doi.org/10.1126/science.abb2169

Ma, X., Guo, X., Richardson, H.E., Xu, T., Xue, L., 2018. POSH regulates Hippo signaling through ubiquitin-mediated expanded degradation. Proceedings of the National Academy of Sciences 201715165. https://doi.org/10.1073/pnas.1715165115

Mao, Y., Tournier, A.L., Hoppe, A., Kester, L., Thompson, B.J., Tapon, N., 2013. Differential proliferation rates generate patterns of mechanical tension that orient tissue growth. EMBO J 32, 2790–2803. https://doi.org/10.1038/emboj.2013.197

Misra, J.R., Irvine, K.D., 2019. Early girl is a novel component of the Fat signaling pathway. PLoS Genet 15, e1007955. https://doi.org/10.1371/journal.pgen.1007955

Morais-de-Sá, E., Vega-Rioja, A., Trovisco, V., St Johnston, D., 2013. Oskar Is Targeted for Degradation by the Sequential Action of Par-1, GSK-3, and the SCF-Slimb Ubiquitin Ligase. Developmental Cell 26, 303–314. https://doi.org/10.1016/j.devcel.2013.06.011

Pan, Y., Heemskerk, I., Ibar, C., Shraiman, B.I., Irvine, K.D., 2016. Differential growth triggers mechanical feedback that elevates Hippo signaling. Proceedings of the National Academy of Sciences 113, E6974–E6983. https://doi.org/oskar

Piekny, A., Werner, M., Glotzer, M., 2005. Cytokinesis: welcome to the Rho zone. Trends in Cell Biology 15, 651–658. https://doi.org/10.1016/j.tcb.2005.10.006

Pietuch, A., Brückner, B.R., Janshoff, A., 2013. Membrane tension homeostasis of epithelial cells through surface area regulation in response to osmotic stress. Biochimica et Biophysica Acta (BBA) - Molecular Cell Research 1833, 712–722. https://doi.org/10.1016/j.bbamcr.2012.11.006

Pinheiro, D., Hannezo, E., Herszterg, S., Bosveld, F., Gaugue, I., Balakireva, M., Wang, Z., Cristo, I., Rigaud, S.U., Markova, O., Bellaïche, Y., 2017. Transmission of cytokinesis forces via E-cadherin dilution and actomyosin flows. Nature 545, 103–107. https://doi.org/10.1038/nature22041

Rauskolb, C., Cervantes, E., Madere, F., Irvine, K.D., 2019. Organization and function of tension-dependent complexes at adherens junctions. Journal of Cell Science 132, jcs224063. https://doi.org/10.1242/jcs.224063

Rauskolb, C., Sun, S., Sun, G., Pan, Y., Irvine, K.D., 2014. Cytoskeletal Tension Inhibits Hippo Signaling through an Ajuba-Warts Complex. Cell 158, 143–156. https://doi.org/10.1016/j.cell.2014.05.035

Ribeiro, P., Holder, M., Frith, D., Snijders, A.P., Tapon, N., 2014. Crumbs promotes expanded recognition and degradation by the SCFSlimb/ -TrCP ubiquitin ligase. Proceedings of the National Academy of Sciences 111, E1980–E1989. https://doi.org/10.1073/pnas.1315508111

Rodrigues-Campos, M., Thompson, B.J., 2014. The ubiquitin ligase FbxL7 regulates the Dachsous-Fat-Dachs system in Drosophila. Development 141, 4098–4103. https://doi.org/10.1242/dev.113498

Roffay, C., Molinard, G., Kim, K., Urbanska, M., Andrade, V., Barbarasa, V., Nowak, P., Mercier, V., García-Calvo, J., Matile, S., Loewith, R., Echard, A., Guck, J., Lenz, M., Roux, A., 2021. Passive coupling of membrane tension and cell volume during active response of cells to osmosis. Proc Natl Acad Sci USA 118, e2103228118. https://doi.org/10.1073/pnas.2103228118

Sansores-Garcia, L., Bossuyt, W., Wada, K.-I., Yonemura, S., Tao, C., Sasaki, H., Halder, G., 2011. Modulating F-actin organization induces organ growth by affecting the Hippo pathway. The EMBO journal 30, 2325–2335.

Sarpal, R., Yan, V., Kazakova, L., Sheppard, L., Yu, J.C., Fernandez-Gonzalez, R., Tepass, U., 2019. Role of α-Catenin and its mechanosensing properties in regulating Hippo/YAP-dependent tissue growth. PLoS Genet 15, e1008454. https://doi.org/10.1371/journal.pgen.1008454

Sinha, B., Köster, D., Ruez, R., Gonnord, P., Bastiani, M., Abankwa, D., Stan, R.V., Butler-Browne, G., Vedie, B., Johannes, L., Morone, N., Parton, R.G., Raposo, G., Sens, P., Lamaze, C., Nassoy, P., 2011. Cells Respond to Mechanical Stress by Rapid Disassembly of Caveolae. Cell 144, 402–413. https://doi.org/10.1016/j.cell.2010.12.031

Stewart, M.P., Helenius, J., Toyoda, Y., Ramanathan, S.P., Muller, D.J., Hyman, A.A., 2011. Hydrostatic pressure and the actomyosin cortex drive mitotic cell rounding. Nature 469, 226–230. https://doi.org/10.1038/nature09642

Stringer, C., Wang, T., Michaelos, M., Pachitariu, M., 2021. Cellpose: a generalist algorithm for cellular segmentation. Nat Methods 18, 100–106. https://doi.org/10.1038/s41592-020-01018-x

Su, T., Ludwig, M.Z., Xu, J., Fehon, R.G., 2017. Kibra and Merlin Activate the Hippo Pathway Spatially Distinct from and Independent of Expanded. Developmental Cell 40, 478-490.e3. https://doi.org/10.1016/j.devcel.2017.02.004

Tokamov, S.A., Su, T., Ullyot, A., Fehon, R.G., 2021. Negative feedback couples Hippo pathway activation with Kibra degradation independent of Yorkie-mediated transcription. eLife 10, e62326. https://doi.org/10.7554/eLife.62326

Uehata, M., Ishizaki, T., Satoh, H., Ono, T., Kawahara, T., Morishita, T., Tamakawa, H., Yamagami, K., Inui, J., Maekawa, M., Narumiya, S., 1997. Calcium sensitization of smooth muscle mediated by a Rho-associated protein kinase in hypertension. Nature 389, 990–994. https://doi.org/10.1038/40187

Wada, K.-I., Itoga, K., Okano, T., Yonemura, S., Sasaki, H., 2011. Hippo pathway regulation by cell morphology and stress fibers. Development 138, 3907–3914. https://doi.org/10.1242/dev.070987

Wang, X., Zhang, Y., Blair, S.S., 2019. Fat-regulated adaptor protein Dlish binds the growth suppressor Expanded and controls its stability and ubiquitination. Proceedings of the National Academy of Sciences 116, 1319–1324. https://doi.org/10.1073/pnas.1811891116

Williams, A.M., Donoughe, S., Munro, E., Horne-Badovinac, S., 2022. Fat2 polarizes the WAVE complex in trans to align cell protrusions for collective migration. eLife 11, e78343. https://doi.org/10.7554/eLife.78343

Xu, J., Vanderzalm, P.J., Ludwig, M., Su, T., Tokamov, S.A., Fehon, R.G., 2018. Yorkie Functions at the Cell Cortex to Promote Myosin Activation in a Non-transcriptional Manner. Developmental Cell 46, 271-284.e5. https://doi.org/10.1016/j.devcel.2018.06.017

Yee, W.B., Delaney, P.M., Vanderzalm, P.J., Ramachandran, S., Fehon, R.G., 2019. The CAF-1 complex couples Hippo pathway target gene expression and DNA replication. MBoC 30, 2929–2942. https://doi.org/10.1091/mbc.E19-07-0387

Yu, J., Zheng, Y., Dong, J., Klusza, S., Deng, W.-M., Pan, D., 2010a. Kibra Functions as a Tumor Suppressor Protein that Regulates Hippo Signaling in Conjunction with Merlin and Expanded. Developmental Cell 18, 288–299. https://doi.org/10.1016/j.devcel.2009.12.012

Yu, J., Zheng, Y., Dong, J., Klusza, S., Deng, W.-M., Pan, D., 2010b. Kibra Functions as a Tumor Suppressor Protein that Regulates Hippo Signaling in Conjunction with Merlin and

Expanded. Developmental Cell 18, 288–299. https://doi.org/10.1016/j.devcel.2009.12.012

Zhang, L., Ward, R.E., 2011. Distinct tissue distributions and subcellular localizations of differently phosphorylated forms of the myosin regulatory light chain in Drosophila. Gene Expression Patterns 11, 93–104. https://doi.org/10.1016/j.gep.2010.09.008

Figure 1

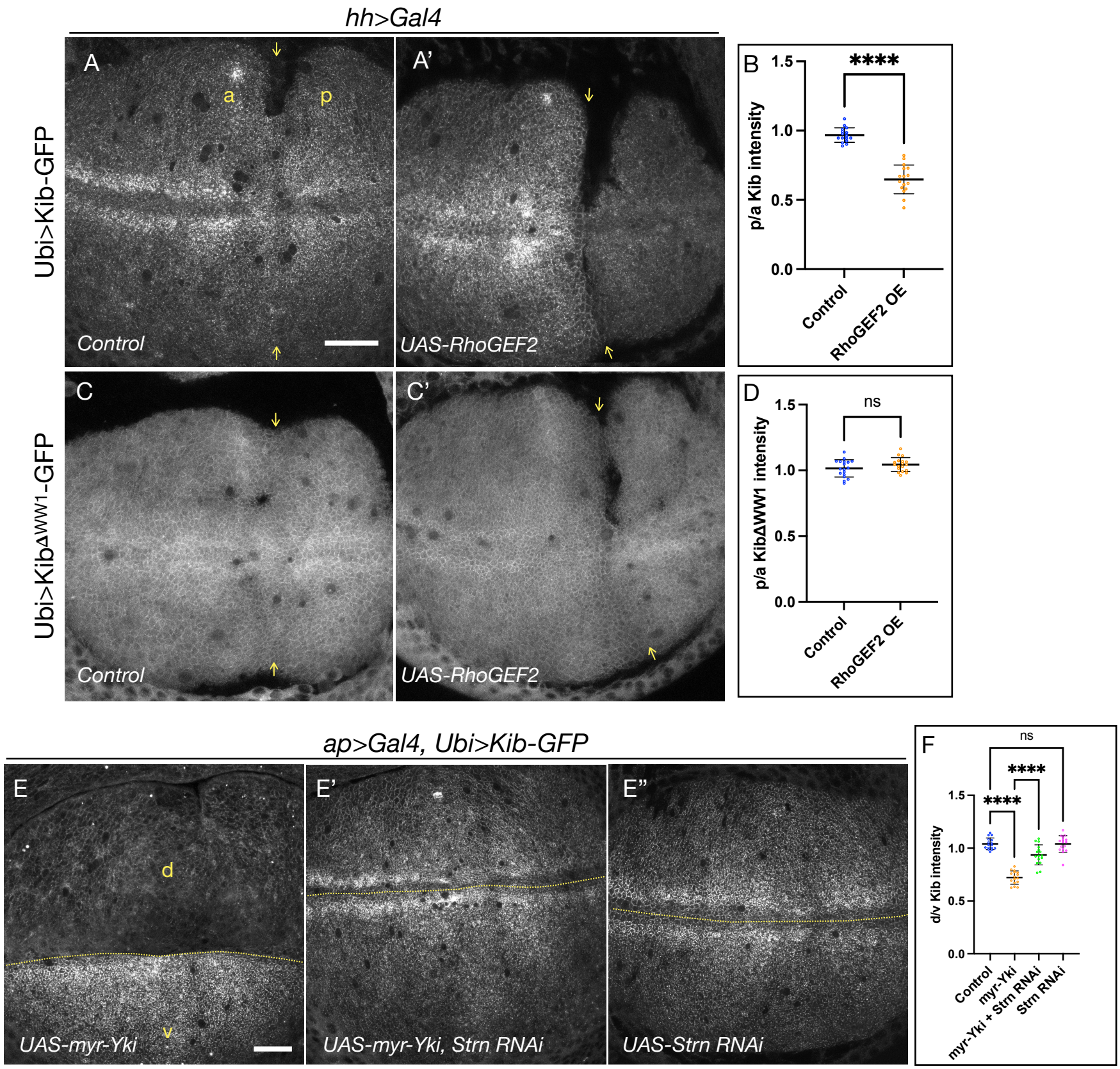
hh>Gal4
Ubi>Kib-GFP
A
a
p
Control
A'
UAS-RhoGEF2
B
****
p/a Kib intensity
1.5
1.0
0.5
0.0
Control
RhoGEF2 OE
Ubi>KibΔWW1-GFP
C
Control
C'
UAS-RhoGEF2
D
ns
p/a KibΔWW1 intensity
1.5
1.0
0.5
0.0
Control
RhoGEF2 OE
ap>Gal4, Ubi>Kib-GFP
E
d
v
UAS-myr-Yki
E'
UAS-myr-Yki, Strn RNAi
E''
UAS-Strn RNAi
F
ns
****
****
d/v Kib intensity
1.5
1.0
0.5
0.0
Control
myr-Yki
myr-Yki + Strn RNAi
Strn RNAi

Figure 2

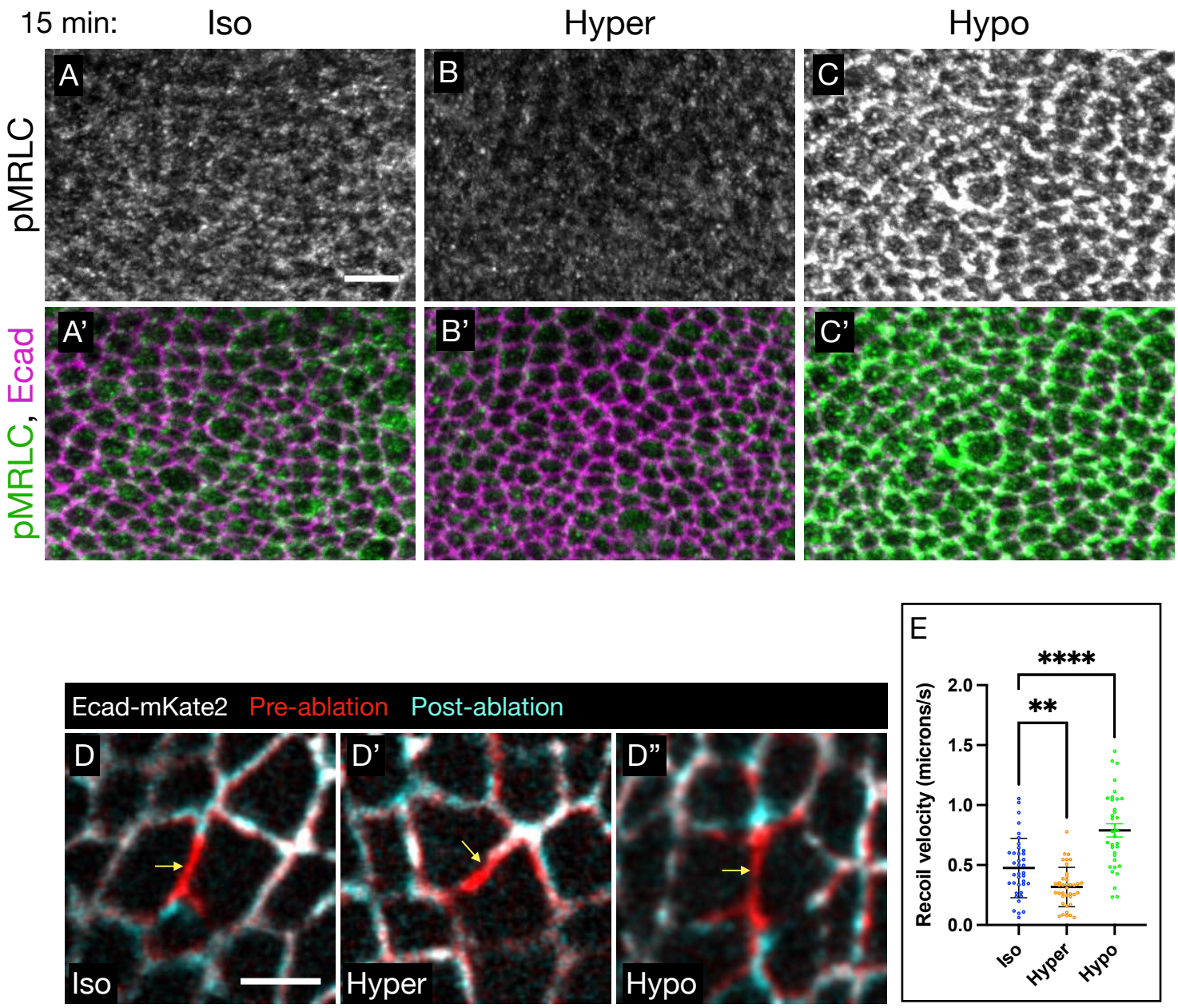
15 min:
Iso
Hyper
Hypo
pMRLC
pMRLC, Ecad
A
B
C
A'
B'
C'
Ecad-mKate2
Pre-ablation
Post-ablation
D
D'
D"
Iso
Hyper
Hypo
E
Recoil velocity (microns/s)
2.0
1.5
1.0
0.5
0.0
**
****
Iso
Hyper
Hypo

Figure 3

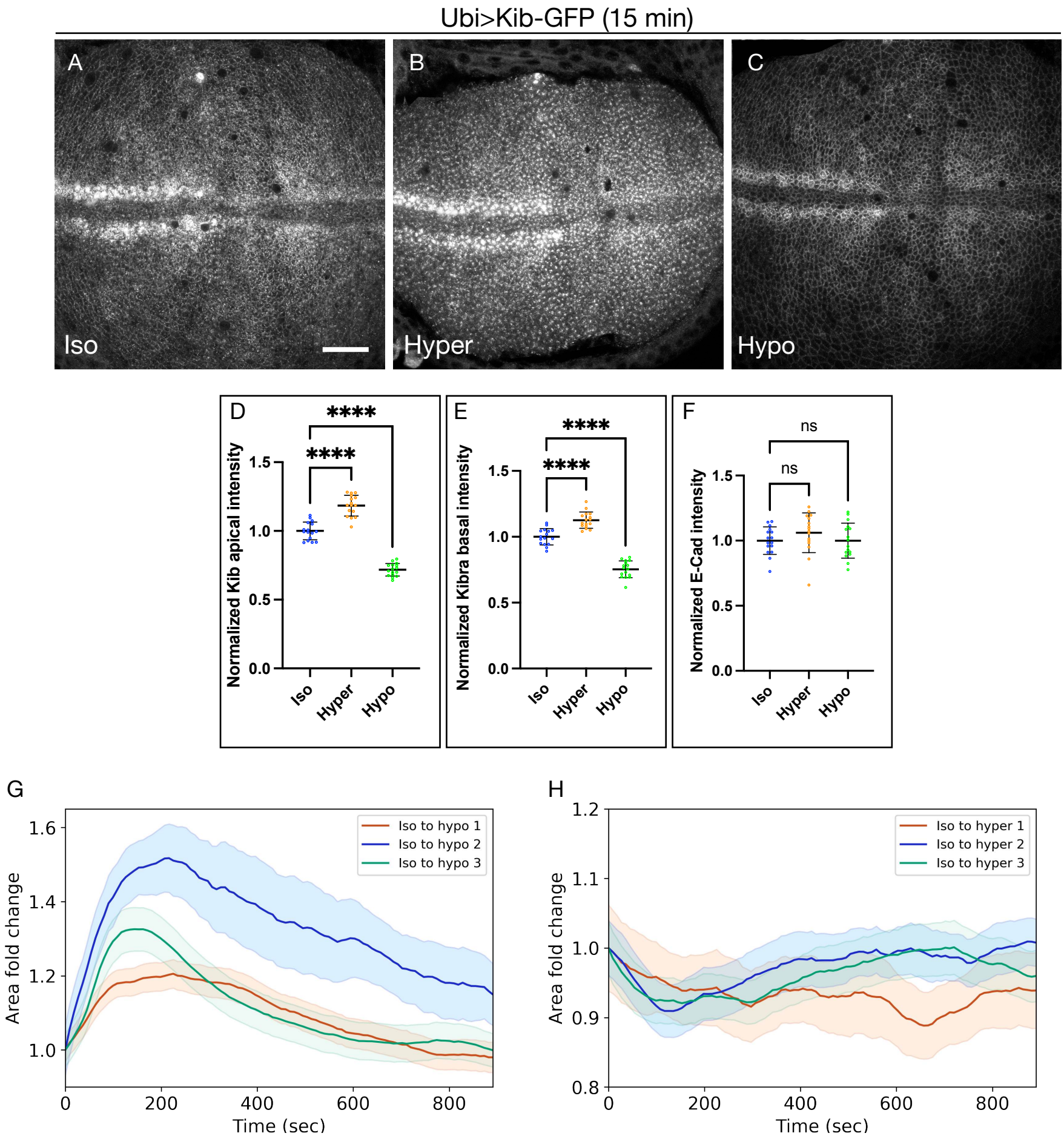
Ubi>Kib-GFP (15 min)
A
Iso
B
Hyper
C
Hypo
D
****
****
Normalized Kib apical intensity
1.5
1.0
0.5
0.0
Iso
Hyper
Hypo
E
****
****
Normalized Kibra basal intensity
1.5
1.0
0.5
0.0
Iso
Hyper
Hypo
F
ns
ns
Normalized E-Cad intensity
1.5
1.0
0.5
0.0
Iso
Hyper
Hypo
G
Iso to hypo 1
Iso to hypo 2
Iso to hypo 3
Area fold change
1.6
1.4
1.2
1.0
0
200
400
600
800
Time (sec)
H
Iso to hyper 1
Iso to hyper 2
Iso to hyper 3
Area fold change
1.2
1.1
1.0
0.9
0.8
0
200
400
600
800
Time (sec)

Figure 4

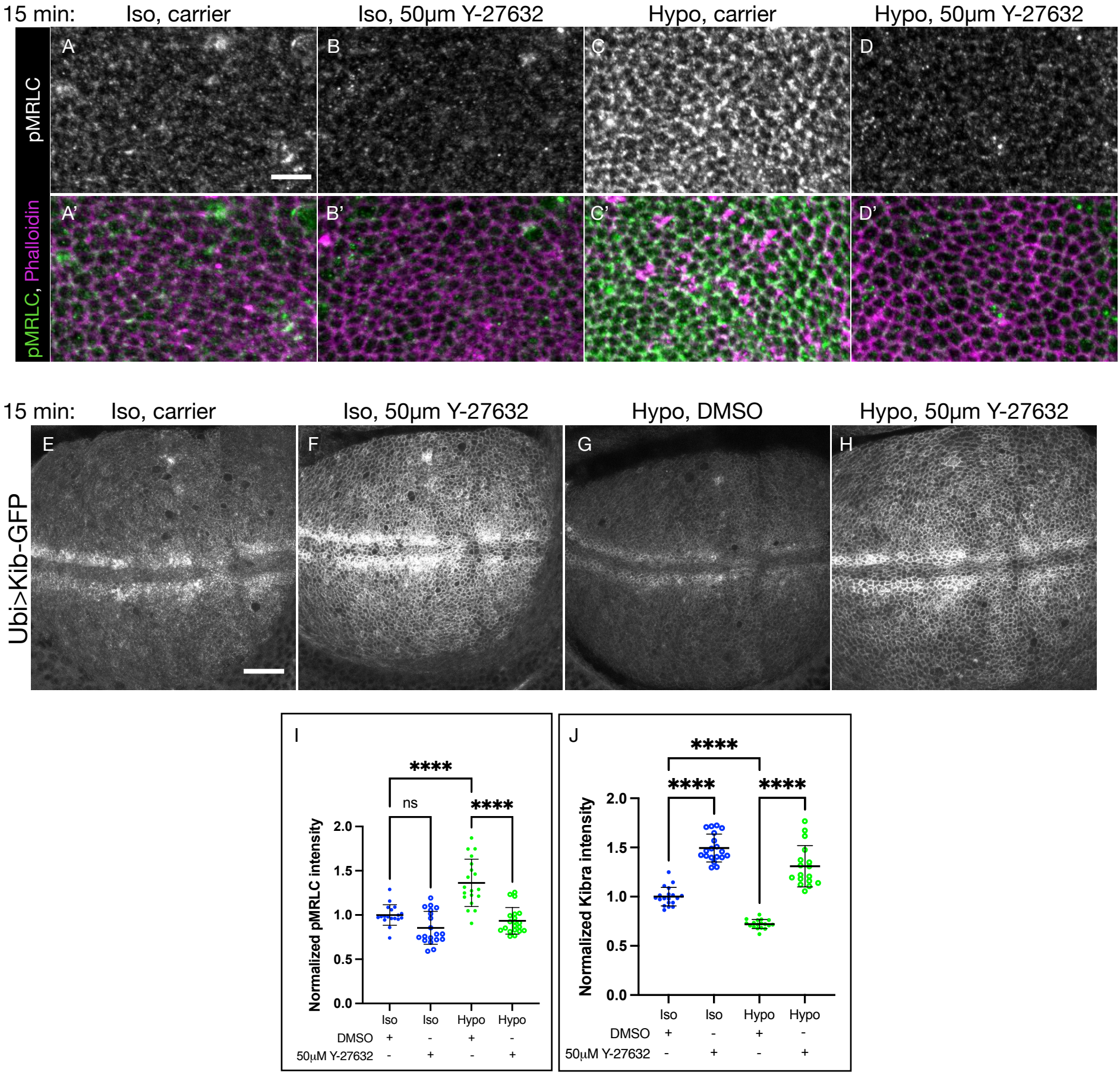
15 min:
Iso, carrier
Iso, 50µm Y-27632
Hypo, carrier
Hypo, 50µm Y-27632
pMRLC
pMRLC, Phalloidin
A
B
C
D
A'
B'
C'
D'
15 min:
Iso, carrier
Iso, 50µm Y-27632
Hypo, DMSO
Hypo, 50µm Y-27632
Ubi>Kib-GFP
E
F
G
H
I
Normalized pMRLC intensity
2.0
1.5
1.0
0.5
0.0
****
ns
****
Iso
Iso
Hypo
Hypo
DMSO + - + -
50µM Y-27632 - + - +
J
Normalized Kibra intensity
2.0
1.5
1.0
0.5
0.0
****
****
****
Iso
Iso
Hypo
Hypo
DMSO + - + -
50µM Y-27632 - + - +

Figure 5

IP:HA

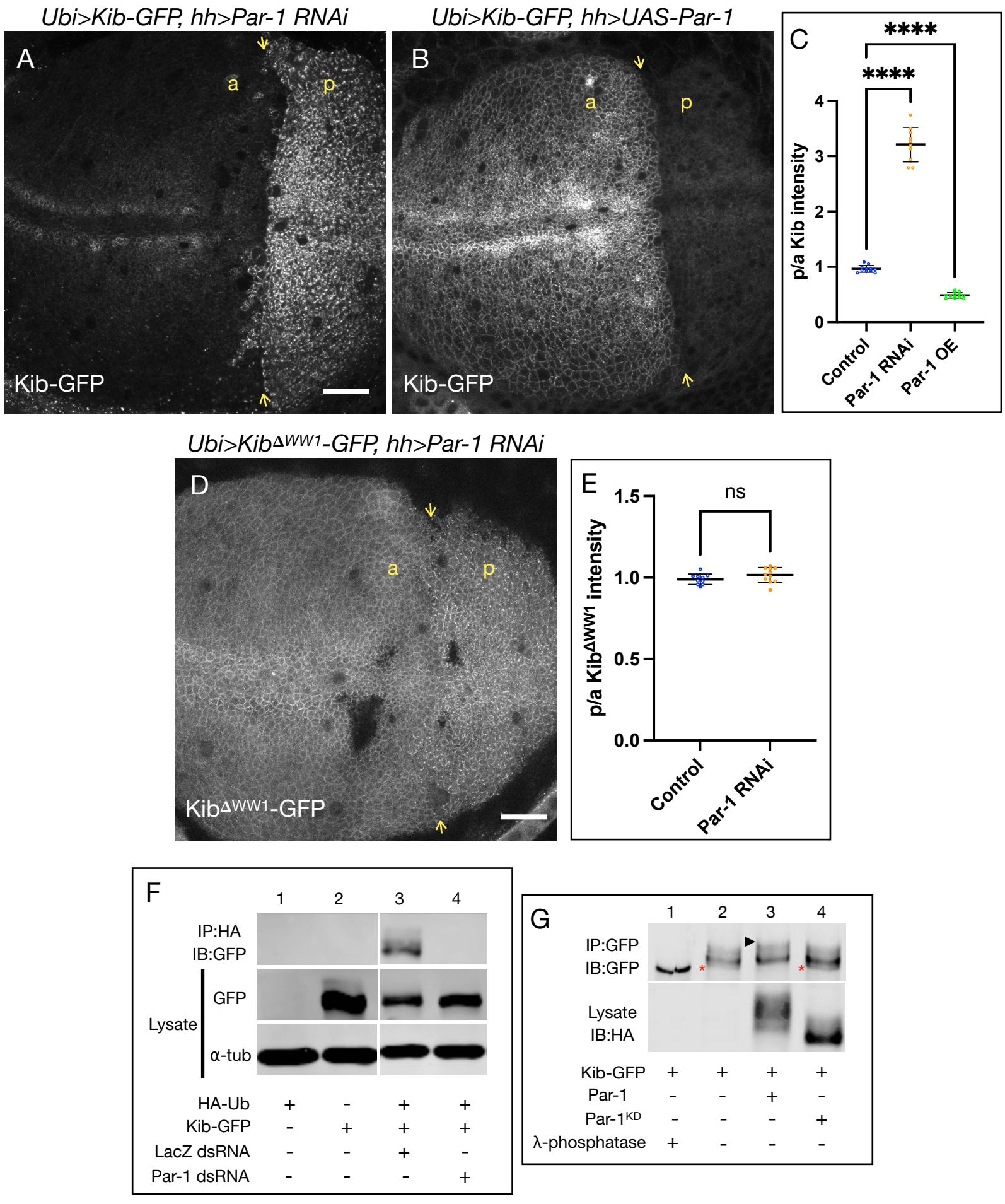

Figure 6

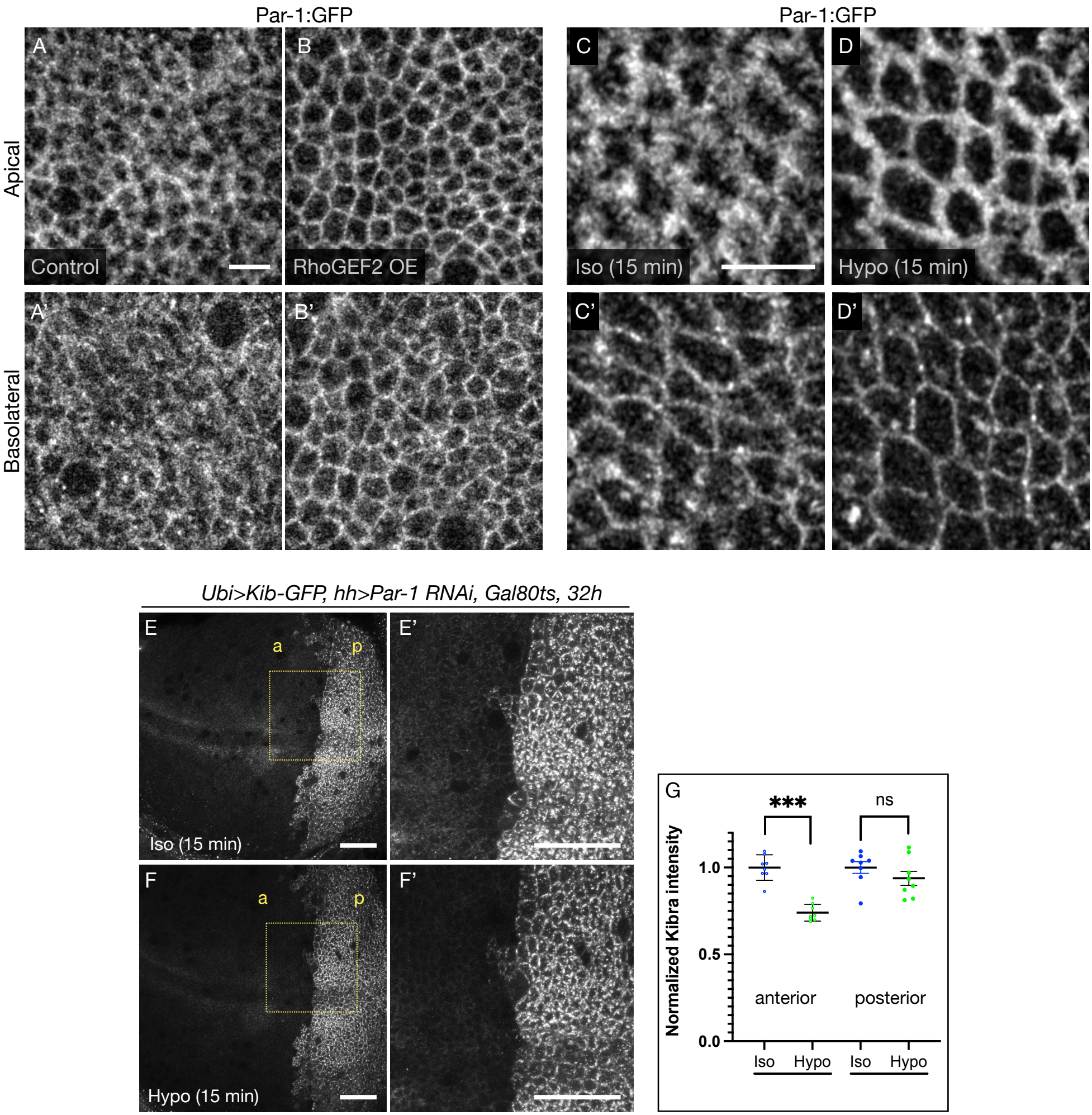
Par-1:GFP
Par-1:GFP
Apical
Basolateral
A
B
C
D
A'
B'
C'
D'
Control
RhoGEF2 OE
Iso (15 min)
Hypo (15 min)
Ubi>Kib-GFP, hh>Par-1 RNAi, Gal80ts, 32h
E
E'
F
F'
a
p
Iso (15 min)
Hypo (15 min)
G
***
ns
Normalized Kibra intensity
1.0
0.5
0.0
anterior
posterior
Iso
Hypo
Iso
Hypo

Figure 1: Cortical tension promotes Kib degradation.
A & B) Compared to control tissues (A), ectopic RhoGEF2 expression results in a significant decrease in Kib abundance (A' & B). Yellow arrows indicate anterior-posterior (a-p) boundary.
C-D) In contrast to wild-type Kib, $Kib^{\Delta WW1}$ is not affected by RhoGEF2 expression.
E-F) Ectopic myr-Yki expression leads to a significant decrease in Kib abundance (E), and depletion of Strn-MLCK suppresses the effect of myr-Yki expression (E'). Depletion of Strn-MLCK alone has no effect on Kib abundance (E''). Dashed lines indicate the dorsal-ventral (d-v) boundary. Scale bars = 20µm.
Plots in (B) and (D) show p/a ratios of mean Kib intensity. Statistical significance was calculated using Mann-Whitney test.
Plot in F shows d/v ratios of mean Kib intensity. Statistical significance was calculated using One-way ANOVA followed by Tukey's HSD test. Unless indicated otherwise throughout the study, data is represented as the mean ± SD and significance values are represented as follows: ****$p \leq 0.0001$, ***$p \leq 0.0001$, **$p \leq 0.001$, *$p \leq 0.05$, ns = not significant.

Figure 2: Changes in osmotic conditions alter myosin activity and cortical tension.
A-C) Compared to isotonic conditions (A-A'), hypertonic conditions lead to a slight decrease in pMRLC (B-B'), whereas hypotonic conditions significantly increase pMRLC signal (C-C'). Scale bar = 5µm.
D-D'') Representative overlay images of Ecad-mKate2 in wing imaginal disc cells pre- (red) and post-ablation of bicellular junctions (arrows) under isotonic (D), hypertonic (D'), hypotonic D'') conditions. Scale bar = 3µm.
E) Quantification of initial junction recoil velocities measured from the ablation experiments. Statistical significance was calculated using One-way ANOVA followed by Tukey's HSD test.

Figure 3: Osmotic shifts affect Kib abundance.

A-C) Compared to isotonic conditions (A), hypertonic shift results in higher Kib abundance (B), while hypotonic shift leads to decreased Kib abundance (C). Scale bar = 20μm.

D-F') Quantification of mean apical Kib-GFP (D), basal Kib-GFP (E), and apical Ecad-mKate2 fluorescence (F). Ecad-mKate2 intensities were measured in the same regions as mean apical Kib-GFP. Statistical significance was calculated using One-way ANOVA followed by Tukey's HSD test.

G & H) Plots of area changes (mean ± SEM) of segmented tissues subjected to hypotonic (G) or hypertonic (H) shifts.

Figure 4: Treatment with Y-27632 raises Kib abundance and reverses the effect of hypotonic shift.

A-D') Staining with the antibody against pMRLC shows a slight decrease in pMRLC staining with Y27632 treatment under isotonic conditions (A-B') and a significant reversal of pMRLC upregulation under hypotonic shift (C-D'). Scale bar = 5µm.

E-H) Compared to control (E), treatment with Y-27632 significantly increases Kib abundance under isotonic conditions (F). Treatment with Y-27632 also reverses the decrease in Kib abundance induced by hypotonic shift (G & H). Scale bar = 20µm.

I) Quantification of normalized mean pMRLC intensities obtained from experiments represented in A-D'.

J) Quantification of normalized mean Kib-GFP intensities obtained from experiments represented in E-H. Statistical significance was calculated using One-way ANOVA followed by Tukey's HSD test.

Figure 5. Par-1 promotes ubiquitin-mediated Kib degradation.
A) Loss of Par-1 in the posterior wing disc compartment leads to a dramatic increase in Kib abundance. Yellow arrows indicate the anterior-posterior (a-p) boundary. Scale bar = 20μm.
B) Ectopic Par-1 expression results in decreased Kib abundance.
C) Quantification of loss or gain of Par-1 function on Kib abundance as a p/a ratio of mean fluorescence intensity. Statistical significance was calculated using One-way ANOVA followed by Tukey's HSD test.
D) Loss of Par-1 does not affect $Kib^{\Delta WW1}$ abundance.
E) Quantification of loss of Par-1 function on $Kib^{\Delta WW1}$ abundance as a p/a ratio of mean fluorescence intensity. Statistical significance was calculated using Mann-Whitney test.
F) Kib immunoprecipitated from cultured S2 cells is normally ubiquitinated when cells are treated with the control LacZ dsRNA (lane 3). Depletion of Par-1 with dsRNA results in a loss of Kib ubiquitination (lane 4).
G) Treatment of Kib samples immunoprecipitated from S2 cells with λ-phosphatase results in non-phosphorylated, faster migrating band (lane 1) relative to phosphorylated, slower migrating bands observed without λ-phosphatase treatment (lane 2). Expression of wild-type Par-1, but not kinase-dead Par-1, leads to increased Kib phosphorylation (lanes 3 & 4). Asterisks indicate non-phosphorylated Kib pool, which disappears upon Par-1 expression. Arrowhead indicates a slower migrating (more phosphorylated) Kib pool.

Figure 6: Cortical tension regulates Kib abundance by modulating cortical Par-1 association.

A & B') Compared to control cells (A-A'), ectopic RhoGEF2 expression leads to tighter Par-1 association with the apical and basolateral cell cortex (B-B'). Scale bar = 5µm.

C & D') Airyscan confocal images showing that compared to isotonic conditions (C-C'), Par-1 becomes more tightly associated with the apical and basolateral cell cortex upon hypotonic shift (D-D'). Scale bar = 5µm.

E-G) Under isotonic conditions, depletion of Par-1 in the posterior compartment (p) leads to a significant increase in Kib levels (E & E', G). Shift to hypotonic conditions leads to a significant decrease in Kib abundance in the anterior region, but only a mild (not statistically significant) decrease in the posterior region where Par-1 was depleted (F & F', G). Scale bars = 20µm. Statistical significance was calculated using Mann-Whitney test.